frontiers | Frontiers in Earth Science

TYPE Original Research
PUBLISHED 30 January 2023
DOI 10.3389/feart.2022.1097551

OPEN ACCESS

EDITED BY
Yun Zhang,
Xi'an University of Science and Technology, China

REVIEWED BY
Baoxu Yan,
Xi'an University of Science and Technology, China
Xuesheng Liu,
Shandong University of Science and Technology, China

*CORRESPONDENCE
Pengfei Jiang,
jiangpengfei@tdkcsj.com

SPECIALTY SECTION
This article was submitted to Structural Geology and Tectonics, a section of the journal Frontiers in Earth Science

RECEIVED 14 November 2022
ACCEPTED 09 December 2022
PUBLISHED 30 January 2023

CITATION
Yao Y, Jiang P, Zhou N and Du E (2023), Study on deformation control of overlying strata in short-wall coordinated filling mining of thick coal seam under aquifer.
Front. Earth Sci. 10:1097551.
doi: 10.3389/feart.2022.1097551

Study on deformation control of overlying strata in short-wall coordinated filling mining of thick coal seam under aquifer

Yinan Yao[1,2], Pengfei Jiang[3]*, Nan Zhou[1,2] and Erbao Du[1,2]

[1]State Key Laboratory of Coal Resources and Safe Mining, China University of Mining and Technology, Xuzhou, Jiangsu, China, [2]School of Mines, China University of Mining and Technology, Xuzhou, Jiangsu, China, [3]Coal Mining Branch, China Coal Research Institute, Beijing, China

The mining of coal resources and the protection of water resources are often in opposition, and this contradiction is more prominent in the mining of thick coal seams due to the difficulty of controlling the overburden deformation. Based on the mining conditions of thick coal seam under the main aquifer of a coal mine in the water shortage area of Northwest China, this paper puts forward the short-wall coordinated filling mining (SCFM) of thick coal seam. The stress analysis of the overall structure consisting of the top and bottom plates, coal pillars and filler at each stage of the mining process was carried out, the length of the short-walled working face suitable for this coal mine was derived, and the key parameters for the mining of the three pan areas of the mine were designed. The analysis results show that the sensitivity of the maximum tensile stress in the roof to the length of the working face is better than the filling rate in the case of short-walled working face arrangement. When the design coal mine working face length is 40 m and the filling rate is 95%, the overburden fissure development height can be controlled to 58.45 m after the whole area of three pan area is retrieved. It is verified by the downhole injection method that the requirement of non-conducting aquifer is satisfied after using SCFM. The research in this paper is of great significance to achieve safe and efficient recovery of coal resources and water conservation under strongly water-rich rock formations.

KEYWORDS

water protection mining, short-wall coordinated filling mining, overburden deformation, fracture development, engineering design

1 Introduction

With its inherent characteristics, coal resources will remain an important source of energy supply for some time in the future, but due to its endowment characteristics and mining methods, most of the mines are facing the problem of massive groundwater loss and ecological environment damage caused by mining activities (Zhang et al., 2014; Fan et al., 2019; Yao et al., 2020). For ecologically fragile areas where water resources are scarce, the decline in groundwater level due to the breakage of aquifers after mining will

make the ecological damage on the surface more serious, and currently backfill mining is widely used as a form of green mining to protect the loss of groundwater resources brought about by the impact of mining (Shen et al., 2021; Zhang et al., 2021). However, it is more difficult to control the overburden for thick seam mining, and the traditional filling mining method often faces the contradiction between the overburden control effect and mining efficiency. Too long working face will result in poor overburden control, while too short will affect mining efficiency (Wen et al., 2019; Tai et al., 2020; Chen et al., 2022). Therefore, the SCFM technology is proposed to control the overburden deformation by reducing the size of the working face together with the filling body filling, which provides a new way for "water conservation mining" (Chi et al., 2019). Systematic study of the influencing factors of overburden deformation of thick coal seam mining under water-bearing seams and establishment of the design process of SCFM parameters are of great significance to improve the safety of thick coal seam mining under water-bearing seams and protect groundwater resources.

Aiming at the filling mining of thick coal seam under aquifer, Deng et al. (2017) proposed a filling mining method of upward slicing longwall-roadway cemented backfilling, and studied the compression performance of cemented backfill materials with different mixing ratios and curing time. The recovery rate and safety of thick coal seam under aquifer are greatly improved by filling mining in layered roadway (Deng et al., 2017). Wen et al. (2022) comparatively analyzed the traditional longwall mining and longwall paste filling mining of thick coal seam, and obtained the key parameters such as mining thickness and filling rate under the critical state of water inrush (Wen et al., 2022). Bai et al. (2018) focused on the effect of backfilling mining under shallow thick coal seams on controlling groundwater loss and reducing surface subsidence, and obtained the optimal ratio of backfilling materials and slurry concentration (Bai et al., 2018).

For the study of the development height of hydraulic fracture zone by backfill mining, Xu et al. (2022) proposed a new method of water-preserved coal mining with long-wall continuous mining and partial filling, and studied the influence of multiple factors on the development height of water flowing fractured zone by analytic hierarchy process, and established a prediction model (Xu et al., 2022). Li et al. (2017) measured and numerically analyzed the development of water-conducting fracture zone in fully mechanized solid filling mining under aquifer, which provided design basis for fully mechanized solid filling (Li et al., 2017). Zhang et al. (2020) studied the controlling effect of short-wall block filling mining method on the development of water flowing fracture and strata movement, established the mechanical development model of water flowing fracture zone, and deduced the development height of water flowing fracture zone (Zhang et al., 2020). Wang (2015) studied the law of water-conducting fracture development in the overburden rock of the Wangerville backfill coal mining method, which provides help to determine reasonable mining parameters for backfill coal mining under water bodies (Wang, 2015).

In summary, there are many analysis and parameter design of overburden control effect of longwall face filling and roadway mining filling, but there is a lack of research on short-wall working face collaborative filling mining and controlling the development of overlying strata deformation and fracture, especially the design of SCFM and the development height of water flowing fractured zone with the whole area mining as the research background.

In this paper, for the requirements of safe mining of coal resources and water resources protection under strong water-bearing strata, the research content of SCFM to control overburden deformation is proposed, and the deformation characteristics of overburden during backfill mining are analyzed in detail to provide reference for similar mines to achieve safe mining of coal resources and water resources protection.

2 Short-wall coordinated filling mining technology

2.1 Engineering background

The study mine is located at the junction of Gansu and Shaanxi provinces in the Yellow River Basin, which is a coal-rich and water-scarce area. The design production capacity of the mine is 5.0 Mt/a, the main mining is $4^{\#}$ coal, the average buried depth is 925.17 m, and the average thickness of the coal seam is 6.67 m. It is a thick coal seam, most of which can be mined, and the structure is simple. The distribution of coal-water dual resources in China and the assignment of coal seams and aquifers in the studied mines are shown in Figures 1A, B, respectively. There are a total of 8 water-bearing rock layers in the overlying rock strata of this coal mine, among which the water-bearing layer of Luohe Group is a strong water-bearing layer, which has a great impact on the mine production. According to the already mined second panel (with similar geological conditions with the third panel) monitoring data show, the average water level of the aquifer in the upper section of the Luohe Formation decreased by 34.95 m during the mining period, and the maximum water inflow of the working face reached 3499.8 m^3/h, with the change curves shown in Figures 1C, D. Therefore, it is very urgent to change the existing mining methods and mining parameters and develop a set of technology suitable for thick coal seam mining under strong aquifer in this mine.

2.2 Short-wall coordinated filling mining

In response to the serious water gushing at the working face during the production of this coal mine, which brings problems

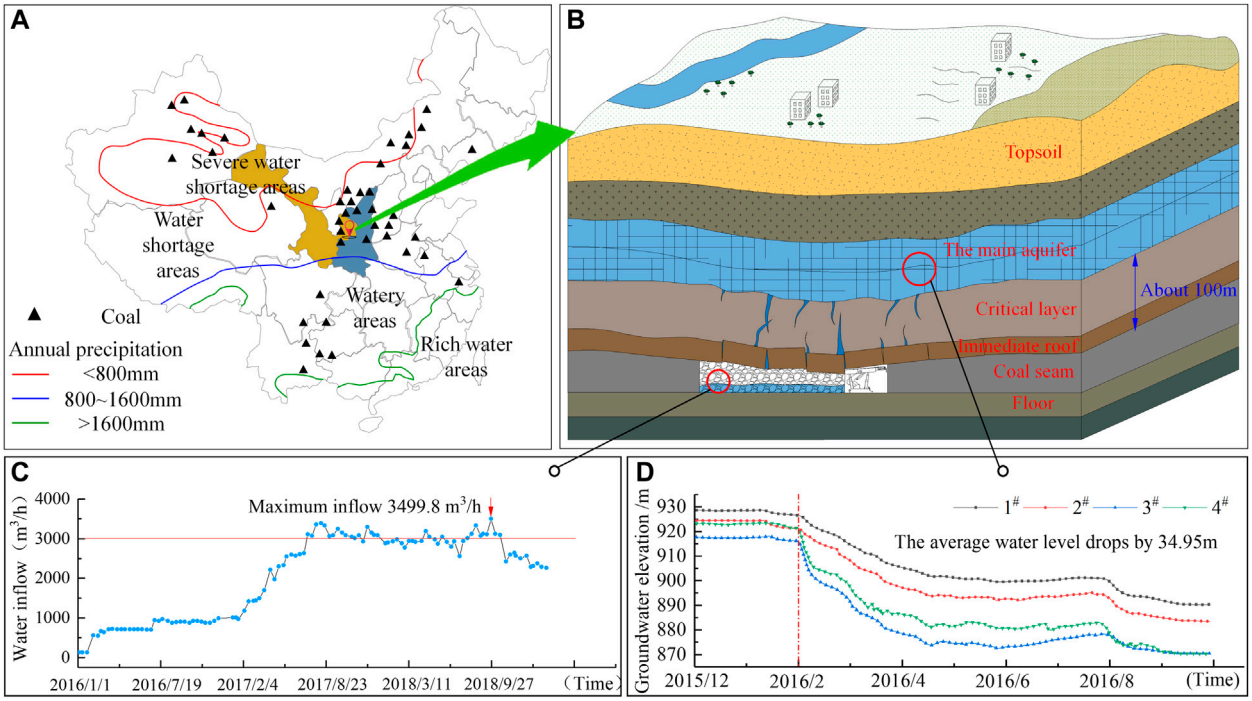

FIGURE 1
Basic information of the mine, **(A)** China coal-water dual resource distribution map, **(B)** Diagram of coal seam and aquifer assignment, **(C)** Working surface water gushing curve graph, **(D)** Water level variation curve of the aquifer in the upper section of the Luohe Formation.

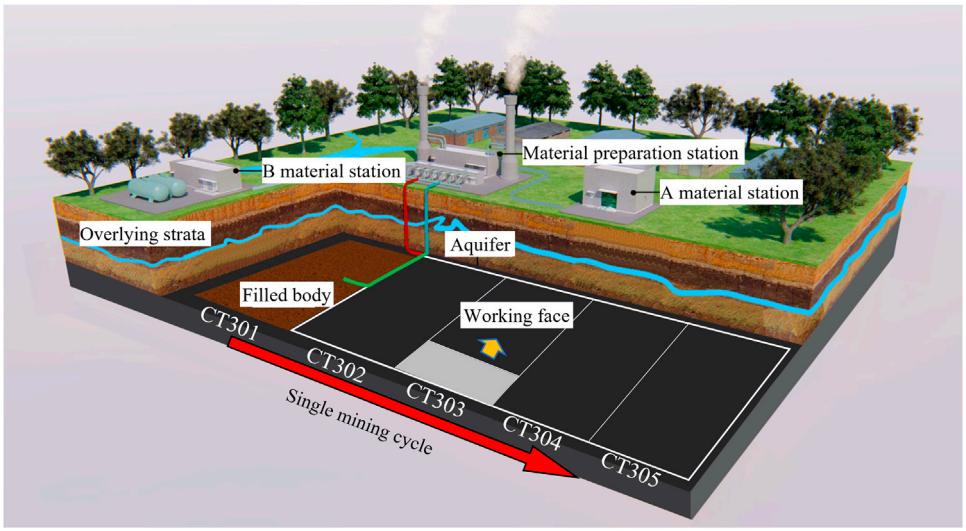

FIGURE 2
The principle diagram of SCFM technology.

to the mine's safety production and water resources protection, the method of SCFM of thick coal seams under strong water-bearing seams is proposed. Ordinary fully mechanized working face length according to the different coal thickness is usually 100–200 m, SCFM than the general fully mechanized mining face length is shorter, usually less than 100 m, for the control of

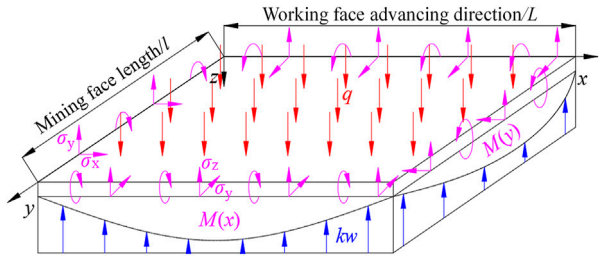

FIGURE 3
Simplified mechanical model of roof in SCFM.

overburden deformation has a certain effect, with high water material filling can be more effective limit overburden deformation space (Wang et al., 2016; Li et al., 2017; Deng et al., 2020). As shown in Figure 2, the SCFM takes a certain number of working faces as a mining cycle (five working faces are taken as an example in the figure). The first step is to form a face production system and finish mining the first face CT301. The second step is to start mining the CT303 face after spacing the coal pillars (i.e., CT302 face) at a certain distance from the first face already mined, and at the same time to fill the CT301 already mined. Step 3: Repeat the above steps after spacing the coal pillar (i.e., CT304 working face) by a certain distance to mine CT305 working face while filling the mined CT303 working face. Step 4: When the mining cycle reaches the designed number of working faces, fill the last working face and start back mining the skipped working faces (i.e., CT302, CT304 working faces) in the order of mining and filling as above until the whole cycle is completed. For the entire mining area, the mining area can be divided into several mining cycles and steps one through four can be repeated to complete the entire area.

3 Key factors of overburden deformation control

The overburden deformation and fracture development after coal seam mining in the working face are mainly affected by factors such as coal seam mining height, working face size, goaf filling rate, lithologic structure, coal seam burial depth and geological structure (Liu et al., 2018; Feng et al., 2021). The mining height is generally determined by the occurrence state of the coal seam, and the size of the working face and the filling rate of the goaf become the main controllable factors. In order to intuitively analyze the damage of the main controllable factors to the roof of the filling coal mining face, the stress model of the roof of the SCFM established to analyze its stress characteristics.

For the study mine, the advance length is determined by the occurrence conditions of coal seams. In most cases, it is greater than 1000 m. The thickness of the immediate roof and the main roof in the overlying strata is about 5 m, and the length of the short-wall working face is generally less than 100 m, preliminary estimate is 50–100 m, according to the definition of thin plate model, short wall face length of 25–400 m can be regarded as thin plate model (Li et al., 2014; Feng et al., 2017). The roof of the overlying strata in the short-wall filling stope can be regarded as a thin plate model, and the filling material is regarded as an elastic foundation. In order to ensure that it does not break under the constraints of the working face size and the filling body, it can be seen as a four-sided clamped plate supported by the high-level rock layer above and supported by the filling body below. The mechanical model of the elastic thin plate is established as shown in Figure 3.

The roof of short-wall filling stope deforms under the joint constraints of working face size and filling body. According to the solution method of elastic mechanics thin plate problem, the internal force problem is transformed into the solution of thin plate deflection equation. The deflection equation of elastic thin plate surface expressed by double sine series is calculated:

$$w(x,y) = \sum_{m=1,3\ldots}^{\infty}\sum_{n=1,3\ldots}^{\infty} A_{mn}\sin\frac{m\pi x}{L}\sin\frac{n\pi y}{l} \tag{1}$$

In the formula, L is the length of the advancing direction of the working face; l is the length of working face; A_{mn} is the generalized coordinate of the bending surface of elastic thin plate. The system composed of stope roof and elastic foundation is regarded as a whole and solved by virtual work principle:

$$w(x,y) = \sum_{m=1,3\ldots}^{\infty}\sum_{n=1,3\ldots}^{\infty} \frac{\frac{Ll}{mn\pi^2}4q + \frac{m\pi}{l}LE_m + \frac{n\pi}{L}lF_n}{\frac{Ll\pi^4}{4}D\left(\frac{m^2}{L^2}+\frac{n^2}{l^2}\right)^2 + \frac{klL}{4}}\sin\frac{m\pi x}{L}\sin\frac{n\pi y}{l} \tag{2}$$

In the formula, the coefficients of bending moment $M(x)$ and $M(y)$ in the form of E_m and F_n Fourier series, $\begin{cases} M(x) = \sum_{m=1,3\ldots}^{\infty} E_m \sin\frac{m\pi x}{L} \\ M(y) = \sum_{n=1,3\ldots}^{\infty} F_n \sin\frac{n\pi y}{l} \end{cases}$; D is bending rigidity; q is uniform load. According to the meanings of elastic modulus, filling rate and elastic foundation coefficient, we can solve the equation of elastic foundation coefficient of the filling body as a function of the filling rate of the mining area $k = \frac{\sigma_0}{h_1(1-\varphi)}$, where σ_0 is the initial stress on the coal seam, h_1 is the mining thickness of the coal seam, and φ is the filling rate of the mining area. By substituting k into Eq. 2, the bending moment expressed by Fourier series appears on the fixed edge, and the plane stress component corresponding to the plate is Eq. 3. By substituting the bending moment $M(x)$ and $M(y)$ in the form of Fourier series into Eq. 3, the maximum tensile stress Eq. 4 on the roof can be obtained, in which σ_x, σ_y and τ_{xy} are the tensile stress of the roof in x and y directions and the shear stress component corresponding to the roof respectively.

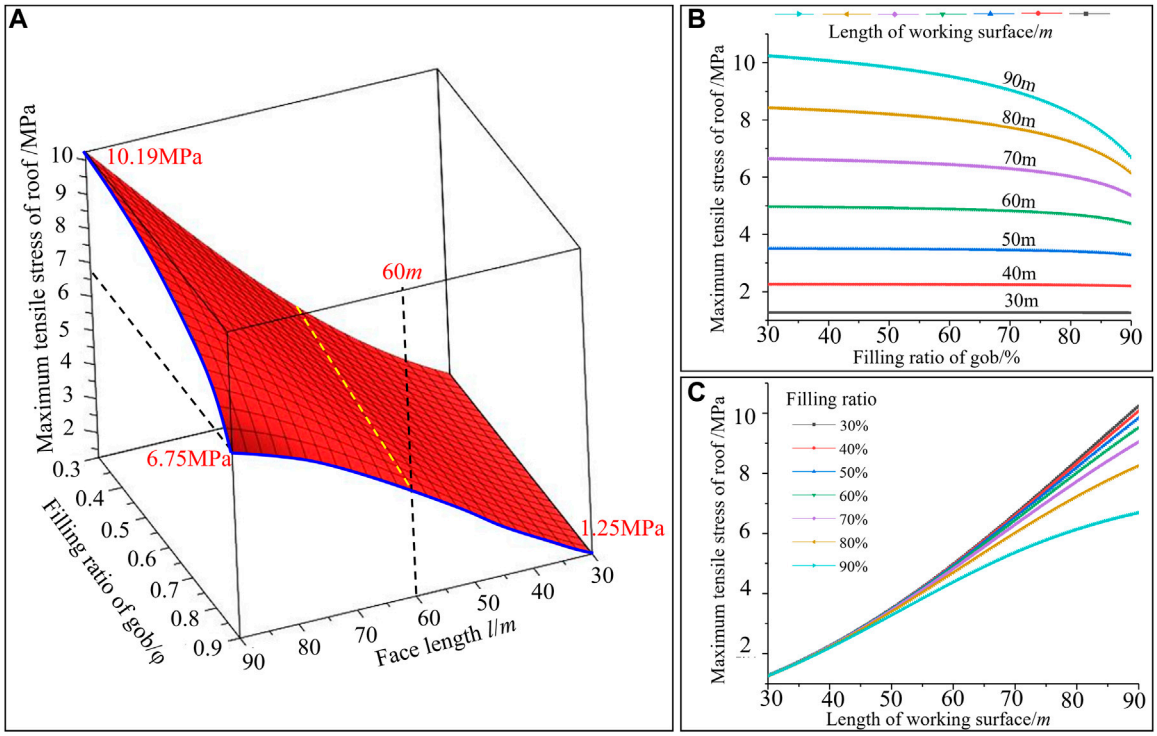

FIGURE 4
Influencing factors of maximum tensile stress of roof, **(A)** The relationship between the maximum tensile stress of the roof and the length of the working face and the filling rate, **(B)** Filling rate, **(C)** Length of working surface.

$$\begin{cases} \sigma_x = \dfrac{12M(x)z}{h^3} \\ \sigma_y = \dfrac{12M(y)z}{h^3} \\ \tau_{xy} = \dfrac{12M(xy)z}{h^3} \end{cases} \tag{3}$$

$$\begin{cases} \sigma_{x\max} = \dfrac{6M(x)}{h^2} = \dfrac{6}{h^2}\sum\limits_{m=1,3\ldots}^{\infty} E_m \sin\dfrac{m\pi x}{L} \\ \sigma_{y\max} = \dfrac{6M(y)}{h^2} = \dfrac{6}{h^2}\sum\limits_{n=1,3\ldots}^{\infty} F_n \sin\dfrac{n\pi y}{l} \end{cases} \tag{4}$$

In order to control the roof without cracks, the critical condition of $\begin{cases} \sigma_{x\max} \le [\sigma_t] \\ \sigma_{y\max} \le [\sigma_t] \end{cases}$ must be satisfied. The coefficients of bending moment $M(x)$ and $M(y)$ expressed by Fourier series can be solved :

$$\begin{cases} \sum\limits_{m=1,3\ldots}^{\infty}\sum\limits_{n=1,3\ldots}^{\infty} \dfrac{\dfrac{Ll}{mn\pi^2}4q + \dfrac{mn\pi}{l}LE_m + \dfrac{m^2\pi}{L}lF_n}{\dfrac{Ll\pi^4}{4}D\left(\dfrac{m^2}{L^2}+\dfrac{n^2}{l^2}\right)^2 + \dfrac{\sigma_0 lL}{4h(1-\varphi)}} = 0 \\ \sum\limits_{m=1,3\ldots}^{\infty}\sum\limits_{n=1,3\ldots}^{\infty} \dfrac{\dfrac{Ll}{mn\pi^2}4q + \dfrac{n^2\pi}{l}LE_m + \dfrac{mn\pi}{L}lF_n}{\dfrac{Ll\pi^4}{4}D\left(\dfrac{m^2}{L^2}+\dfrac{n^2}{l^2}\right)^2 + \dfrac{\sigma_0 lL}{4h(1-\varphi)}} = 0 \end{cases} \tag{5}$$

According to the geological conditions of the SCFM face in the third panel of the mine, the average thickness of the coal seam is 6.67 m, the average dip angle is 8°. The basic roof of the overlying strata is fine-grained sandstone, the bending stiffness D is 1.64×10^{12} N·m, the elastic modulus E is 14.3 GPa, the Poisson's ratio μ is 0.3, the thickness h is 3.79 m, the length L of the working face is 375 m, and the length of the working face is to be determined. The uniform load of the overlying strata of the basic roof q is calculated to be 0.17 MPa. In order to simplify the calculation of the plate model, the first two terms representing the Fourier coefficients of the fixed edge bending moment are selected and substituted into the above parameters to solve the Fourier coefficients E_1, E_3, F_1 and F_3 corresponding to the bending moment :

$$\begin{cases} E_1 = -\dfrac{(660.37\times(6.89\times10^{14}l^4\varphi - 3.51\times10^{16}l^4 + 1.81\times10^{20}l^2(\varphi-1) + 8.60\times10^{25}(\varphi-1))}{1.29\times10^{14}l^4\varphi - 4.33\times10^{15}l^4 + 1.30\times10^{19}l^2(\varphi-1) + 2.54\times10^{24}(\varphi-1)} \\ E_3 = \dfrac{(220.12\times(3.06\times10^{15}l^4\varphi + 4.50\times10^{15}l^4 + 9.77\times10^{20}l^2(\varphi-1) + 6.05\times10^{25}(\varphi-1))}{1.29\times10^{14}l^4\varphi - 4.33\times10^{15}l^4 + 1.30\times10^{19}l^2(\varphi-1) + 2.54\times10^{24}(\varphi-1)} \\ F_1 = -\dfrac{2.07\times10^{21}\times(20992l^2\varphi - 1.72\times10^5l^4 + 1.30\times10^9l^2(\varphi-1) + 9.11\times10^{13}(\varphi-1))}{(1.29\times10^{14}l^4\varphi - 4.33\times10^{15}l^4 + 1.30\times10^{19}l^2(\varphi-1) + 2.54\times10^{24}(\varphi-1))} \\ F_3 = 0 \end{cases} \tag{6}$$

Substituting Eq. 6 into Eq. 4, the relationship between the maximum tensile stress of roof and the length and filling rate of working face can be obtained. In order to intuitively analyze the

relationship between the maximum tensile stress of roof and the two, Eq. 7 is further processed and drawn into Figure 4.

$$\sigma_{t\max} = \frac{34.03l^2\left(6.89\times10^{14}l^4\varphi - 3.51\times10^{16}l^4 + 1.81\times10^{20}l^2(\varphi-1) + 8.60\times10^{25}(\varphi-1)\right)}{1.29\times10^{14}l^4\varphi - 4.33\times10^{15}l^4 + 1.30\times10^{19}l^2(\varphi-1) + 2.54\times10^{24}(\varphi-1)} + \frac{11.34l^2\left(3.06\times10^{15}l^4\varphi + 4.50\times10^{15}l^4 + 9.77\times10^{20}l^2(\varphi-1) + 6.05\times10^{25}(\varphi-1)\right)}{1.29\times10^{14}l^4\varphi - 4.33\times10^{15}l^4 + 1.30\times10^{19}l^2(\varphi-1) + 2.54\times10^{24}(\varphi-1)} \quad (7)$$

From the analysis in Figure 4A, it can be seen that when the filling rate is 90%, the maximum tensile stress of the roof decreases from 6.75 to 1.25 MPa during the reduction of the working face length from 90 m to 30 m, and the reduction rate reaches 81.48%. When the working face length is 90 m, the maximum tensile stress of the roof decreases from 10.19 to 6.75 MPa in the process of decreasing the filling rate from 30% to 90%, and the decrease is 33.95%. It is easy to know that the maximum tensile stress of the roof in the short-wall filling mining working face is more sensitive to the length of the working face than the filling rate of the goaf, i.e., the length of the working face has a greater influence on the maximum tensile stress of the roof.

From the analysis of Figures 4B, C, it can be seen that the maximum tensile stress in the roof slab decreases with the increase of the filling rate, but the reduction rate is affected by the length of the working face, and the critical value is roughly 60 m. When the working face length is greater than 60m, the effect of increasing filling rate on the reduction of maximum tensile stress in the roof is more obvious, and this effect increases with the increase of working face length. When the working face length is 60 m, 70 m, 80 m and 90 m respectively, the maximum tensile stress reduction of the roof corresponding to the increase of filling rate from 30% to 90% is 33.95%, 25.61%, 18.52%, and 8.40% respectively. In contrast, the maximum tensile stress of the roof plate decreases very little with the increase of the filling rate when the working face length is less than 60 m, and even remains basically unchanged.

At the same time, the maximum tensile stress in the roof increases significantly with the increase of the working face length regardless of the filling rate. However, when the filling rate is low, the roof tensile stress changes significantly with the length of the working face, and the increase slows down gradually with the increase of the filling rate. When the filling rate of the goaf is 60%, 70%, 80% and 90%, the increase of maximum tensile stress of the roof corresponding to the increase of the working face length from 40 m to 90 m is 352.38%, 328.57%, 290.48%, and 221.43% respectively.

To sum up, under the layout of short-wall filling mining face, the sensitivity of the maximum tensile stress of the roof to the length of the working face is better than the filling rate. In the design process of mining parameters, the length of the working face should be taken as the main factor to control the development of roof cracks, but the filling must be used to prevent the development of cracks caused by the slow deformation of the roof.

4 Working face design based on elastic foundation coefficient

It can be seen from the above section that the length of the working face plays a key role in controlling the maximum tensile stress of the roof in the main controllable factors of SCFM. According to the operation process of SCFM, taking five working faces of single mining cycle as an example, the stress analysis of the interaction system composed of coal body, filling body and roof in each mining step is carried out. It is easy to know that the deformation of overlying strata is always controlled by the three mining units of the current mining face and the left and right adjacent mining affected areas. Therefore, the design principle of working face length is that the roof control range of three working units should be greater than the stress concentration area. When the solid coal is recovered by filling, the combination of roof and filling body forms a coupling system of stress and deformation. In order to facilitate the analysis, the three operating units are regarded as the foundation synergy with different elastic coefficients to jointly control the roof subsidence.

In a single mining cycle, the supporting capacity of the overall structure composed of roof and floor, coal pillar and filling body to the overlying strata is related to the mining state of different stages of the working face. The following is an analysis of the three basic structures formed during the single mining cycle, and then the different states of the combination of coal pillar and filling body during the whole mining period are analyzed.

(1) Structure 1:

Structure 1 consists of a filling body and its two adjacent working faces, whose stress state under the action of roof and floor is shown in Figure 5. The filling body is in the stage of being compacted and sunk, and the small elastic foundation coefficient causes the stress of the two adjacent working faces to rise. The relationship between the three units and the roof is established by the elastic foundation theory, as shown in Eq. 8.

$$2\int_0^{L_1} k_1 w_1(x,y)dy + \int_{L_1}^{l+L_1} k w_2(x,y)dy = q_2(2L_1 + l) \quad (8)$$

In the formula, k_1 is the elastic foundation coefficient of coal pillar unit; k is the equivalent elastic foundation coefficient; q_2 is the load of coal pillar and filling body; w_1 and w_2 are the deformation of coal pillar and filling body unit; L_1 is the length of working face to be mined; l is the length of the mined face.

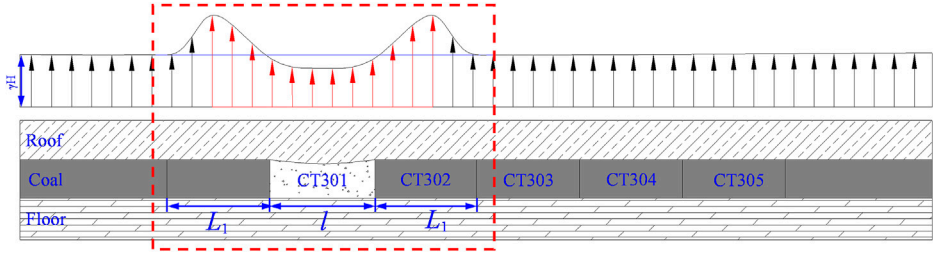

FIGURE 5
Structure 1 stress analysis diagram.

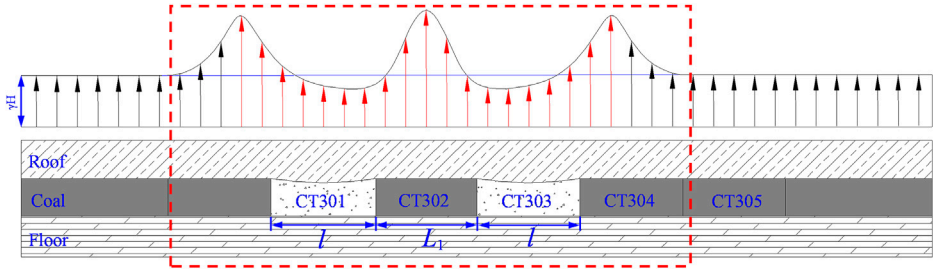

FIGURE 6
Structure 2 stress analysis diagram.

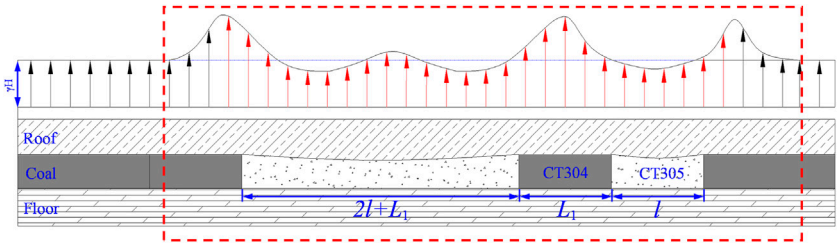

FIGURE 7
Structure 3 stress analysis diagram.

Solving Eq. 8, the relationship between the length of working face and elastic foundation coefficient can be expressed as:

$$L_1 = \frac{E_0}{q_2 h_1}\int_0^{L_1} w_1(x,y)dy \tag{9}$$

In the formula, E_0 is the elastic modulus of filling body; h_1 is the height of filling body.

(2) Structure 2:

Structure 2 is composed of two filling bodies sandwiched by a working face to be mined. The stress state of structure 2 under the action of roof is shown in Figure 6. The working face to be mined temporarily becomes the main bearing body in the structure at this stage, and the stress increases obviously. The relationship between the three units and the roof is established by the elastic foundation theory as shown in Eq. 10.

$$2\int_{L_1}^{l+L_1} kw_2(x,y)dy + \int_{L_1+l}^{2L_1+l} k_1 w_1(x,y)dy = q_2(2l+L_1) \tag{10}$$

By solving the Eq. 10, the relationship between the working face length and the elastic foundation coefficient in the case of structure two can be expressed as follows:

$$L_1 = \frac{E_0}{q_2 h_1}\int_{L_1+l}^{2L_1+l} w_1(x,y)dy \tag{11}$$

(3) Structure 3:

As shown in Figure 7, the third structure is a working face to be mined plus two asymmetric filling bodies, that is, the size of the filling areas on both sides is inconsistent, resulting in an asymmetric increase in the stress of the working face to be mined. The relationship between the three units and the roof is established by the elastic foundation theory as shown in Eq. 12.

$$\int_{L_1}^{2L_1+2l} kw_2(x,y)dy + \int_{2L_1+2l}^{3L_1+2l} k_1 w_1(x,y)dy + \int_{3L_1+2l}^{3L_1+3l} kw_2(x,y)dy = q_2(3l+2L_1) \tag{12}$$

Solving Eq. 12, the relationship between the length of working face and elastic foundation coefficient can be expressed as:

$$L_1 = \frac{E_0}{q_2 h_1}\int_{2L_1+2l}^{3L_1+2l} w_1(x,y)dy \tag{13}$$

From the process flow of SCFM, it can be seen that different mining stages in the mining area during the whole mining period are the combination of the above three conditions. By combining the above three conditions, the stress conditions of different stages in the whole mining process can be obtained, and then the influence of the length of the working face on the elastic foundation coefficient can be obtained, and the reasonable distance between the length of the working face L_1 and l can be analyzed. According to the elastic foundation coefficient and the force balance condition, in order to ensure that the stress appears within a reasonable range, the interval distance between the first and the fifth mining face is respectively (14)–(18).

$$L_1 = \frac{E_0}{q_2 h_1}\int_{0}^{L_1} w_1(x,y)dy \tag{14}$$

$$L_1 = \frac{E_0}{3q_2 h_1}\left[\int_{0}^{L_1} w_1(x,y)dy + \int_{L_1+l}^{2L_1+l} w_1(x,y)dy + \int_{2(L_1+l)}^{3L_1+2l} w_1(x,y)dy\right] \tag{15}$$

$$L_1 = \frac{E_0}{4q_2 h_1}\left[\int_{0}^{L_1} w_1(x,y)dy + \int_{L_1+l}^{2L_1+l} w_1(x,y)dy + \int_{2(L_1+l)}^{3L_1+2l} w_1(x,y)dy + \int_{3(L_1+l)}^{4L_1+3l} w_1(x,y)dy\right] \tag{16}$$

$$L_1 = \frac{E_0}{3q_2 h_1}\left[\int_{0}^{L_1} w_1(x,y)dy + \int_{L_1+3l}^{2L_1+3l} w_1(x,y)dy + \int_{2L_1+4l}^{3L_1+4l} w_1(x,y)dy\right] \tag{17}$$

$$L_1 = \frac{E_0}{2q_2 h_1}\left[\int_{0}^{L_1} w_1(x,y)dy + \int_{L_1+5l}^{2L_1+5l} w_1(x,y)dy\right] \tag{18}$$

From the above-mentioned analysis of the workface spacing distance elastic foundation expressions for each recovery step, it can be seen that the stress is greatest at the time of the fourth recovery operation and the highest requirements for workface spacing. And the structure consisting of the filling area and the working face to be mined varies with the size of the working face. When the length of the working face is not consistent, it is more conducive to the release of the support pressure, but it will have a negative impact on the mining process. In order to balance the requirements for overlying rock control and to coordinate the production process to improve mining efficiency, the distance with the highest requirements for workface spacing was chosen as the workface length. Substituting the specific parameters of the study mine in Section 2, and considering a certain safety factor, we get that the roof control range of the three operating units is larger than the stress concentration zone when the length of the fourth recovery operating face is 40 m.

5 SCFM overburden hydraulic conductivity fracture development

5.1 Overburden hydraulic conductivity fracture peak point analysis

Generally the overburden rock appears collapse, fracture, bending and other characteristics from bottom to top after the coal seam is retrieved, and the development height of the fracture zone is directly related to whether the overburden aquifer can be conducted (Miao et al., 2011; Liu et al., 2017). The rock strata in the range of fractured zone have the characteristics of maintaining the original layer state, but the hard rock strata in this range are easy to break and crack, which makes the water seepage phenomenon, while the soft rock strata have good toughness and allow large deformation, which has a good barrier effect on the seepage of water (Xie et al., 2021). After the rupture of the hard roof in the lower side, under the combined action of stress release and the weak rock layer above, the fracture of the overlying rock may terminate here. The critical breaking height of the soft rock layer in the overlying rock layer is regarded as the peak point of the development of water flowing fracture (Liu et al., 2019; Li et al., 2021).

The soft rock stratum is bent and sunk by the support of the coal walls on both sides, and the critical rupture position is related to the span between the coal walls. When the span is large, the maximum curvature of soft rock occurs above the side of coal wall. When the span is small, the maximum curvature of soft rock occurs right above the middle of the mining area. In this paper, the soft rock stratum is regarded as a fixed beam model, as shown

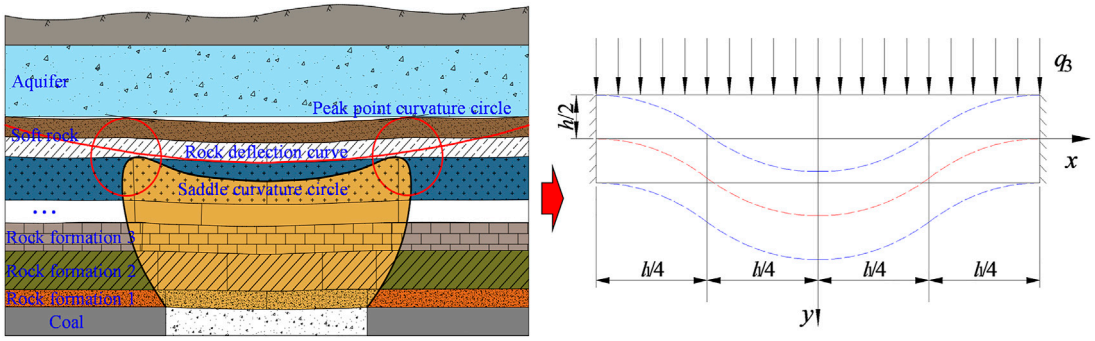

FIGURE 8
Mechanical model of solid support beam for overlying soft rock formations.

in Figure 8, and the peak point of overburden fracture development after the whole period of SCFM is analyzed.

The bending deflection equation of the fixed beam model is :

$$w_3 = a_1\left(1+\cos\frac{2\pi x}{l_1}\right)+a_2\left(1+\cos\frac{6\pi x}{l_1}\right) +\cdots+a_n\left(1+\cos\frac{(2n-1)2\pi x}{l_1}\right) \tag{19}$$

In the formula, w_3 and l_1 are the deflection and span of the fixed beam in the overlying weak rock stratum respectively. The effective load q_3, elastic modulus E_2 and inertia moment I to z axis of the weak strata of overlying strata are respectively brought into Eq. 19 to obtain:

$$w_3 = \sum_{i=1}^{n}\frac{q_3 l_1^4}{\left[(2n-1)2\pi\right]^3(2n-1)\pi E_2 I}\left(1+\cos\frac{(2n-1)2\pi x}{l}\right) \tag{20}$$

Based on the deformation deflection curve of the fixed beam obtained above, the maximum deflection of the fixed beam model of overburden rock is:

$$w_{3\,\max} = w_3|_{x=\frac{l_1}{2}} = \frac{4q_3 l_1^4}{\pi^4 E_2 I} = 0.041\frac{q_3 l_1^4}{E_2 I} \tag{21}$$

At the same time, the rotation angle equation of fixed beam is:

$$\theta = \frac{\mathrm{d}w_3}{\mathrm{d}x} = \sum_{i=1}^{n}\frac{-q_3 l_1^2}{(2n-1)^3\pi^3 E_2 h_2^3}\sin\frac{(2n-1)2\pi x}{l_1} \tag{22}$$

The curvature equation of fixed beam is:

$$\frac{1}{\rho} = \frac{\mathrm{d}^2 w_3}{\mathrm{d}x^2} = -\sum_{i=1}^{n}\frac{6q_3 l_1}{(2n-1)^2\pi^2 E_2 h_2^3}\cos\frac{(2n-1)2\pi x}{l_1} \tag{23}$$

In the formula, ρ is the radius of curvature of the soft rock layer. Under the condition of bending deformation of soft rock stratum, the smaller the radius of curvature, that is, the greater the curvature, the greater the tensile deformation. Therefore, the maximum value of the curvature equation of the clamped beam in the soft rock layer of Eq. 23 can be obtained and the deformation at this position (generally 2 mm/m) can still maintain the integrity of the entire soft rock layer, that is, the critical span can be obtained (Zhao et al., 2018; Li, 2019). The allowable limit span under the condition of maximum horizontal deformation of soft rock stratum is:

$$l_1 = \frac{2E_2 h_2^2}{375 q_3} \tag{24}$$

The distance from the upper and lower boundaries of the soft rock strata to the roof of the coal seam is the height of the water-conducting fracture development, and this position is the peak point at different positions of the water-conducting fracture development.

5.2 Overburden fracture development height under the whole area recovery condition

The dip direction of the third panel of the mine is more than 1000 m, and the distance from the boundary of the second and third panels to the boundary of the third and fourth panels is about 700 m in the strike direction. The number of working faces and mining size in the strike direction should be designed according to the allowable development height of the water flowing fracture in the overlying strata. The development height of the water flowing fracture must also meet the control requirements after the completion of the mining in the whole area.

The main aquifer in the third panel is the Luohe Formation aquifer, and the main aquifuge is the Anding Formation aquifuge. Through the analysis of drilling data, it can be seen that the thickness of the effective interval between the coal seam roof and the lower boundary of the Luohe Formation aquifer is 100 m, and the thickness of the Anding Formation aquifuge is about 35 m. Considering a certain safety factor, it is considered safe to control the

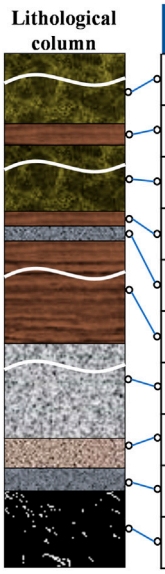

Name of stratum	Thickness /m	Density /kg·m^{-3}	Elastic modulus/MPa	Compressive strength/MPa	Tensile strength/MPa
Sandy mudstone	17.24	2100	1080	25.1	3.10
Coarse Sandstone	1.50	2590	19650	78	3.91
Sandy mudstone	9.80	2100	1080	25.1	3.10
Coarse Sandstone	1.00	2590	19650	78	3.91
mudstone	1.00	2050	6840	30	2.37
Coarse Sandstone	23.08	2590	19650	78	3.91
medium grained sandstone	17.03	2380	21830	70	3.08
fine-sandstone	3.79	2150	14270	50	3.20
mudstone	1.25	2050	6840	30	2.37
4#coal	6.67	1900	4830	10	0.87

FIGURE 9
Mechanical parameters of overlying rock layers in three panels.

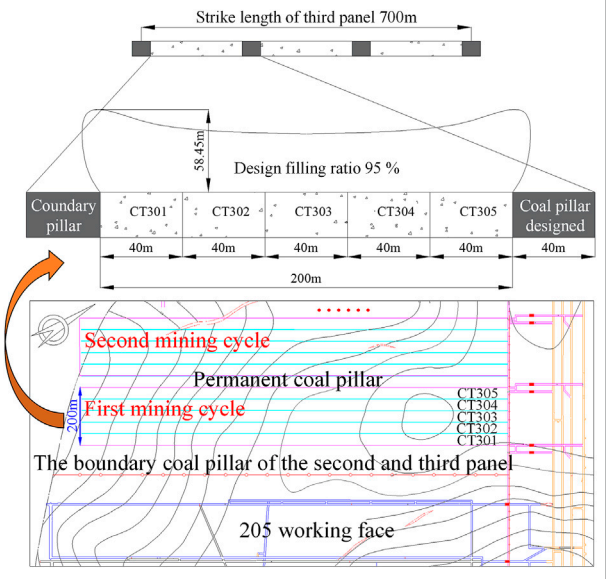

FIGURE 10
Parameter design diagram of the three-panel area of the mine.

development height of the overburden rock fracture within 65 m. The distribution of overlying soft rock strata in the third panel is shown in Figure 9.

According to the height of overburden deformation and fracture development in the mine can't exceed 65 m, it is concluded that the 9th layer of sandy mudstone in the overlying strata is the critical soft rock layer. The critical span obtained under the condition of critical tensile deformation is the maximum mining width allowed after the whole mining of the third panel. Through the Eq. 25, the load q_3 of the 9th layer of soft rock is 0.78 Mpa.

$$(q_3)_k = \frac{E_2 h_2^3 \sum_{k=1}^{s} h_k \gamma_k}{\sum_{k=0}^{s} E_k h_k^3} \tag{25}$$

Substitute the actual parameters of the 9th layer of soft rock formation into the above Eq. 24 and design the fixed beam according to the requirement that the width of the solid support beam is 1/2–1/3 of the height and the height is 1/10–1/12 of the span, and the load is the line load along the span direction, and take the maximum span of 200 m with certain safety factor. The strike distance of the whole mining area between the boundary coal pillars in the third panel is 693 m. It can be seen that the 9th soft rock layer will be destroyed and produce cracks after the whole mining area is mined. Therefore, according to the previous analysis, the third panel is designed as follows.

As shown in Figure 10, the strike length of the three-panel area of the study mine is approximately 700 m, which far exceeds the critical span of 200 m for the 9th soft rock layer, so the critical span of 200 m is used as a mining cycle, where each working face is 40 m long and divided into 5 working faces. In order to ensure that the overburden deformation fracture development is still within the control range after the mining range is increased, a

TABLE 1 Drilling design parameters.

Number	Inclination/°	Hole depth/m	Vertical depth/m	Horizontal distance/m
1#	50	130.54	100	83.91
2#	55	122.08	100	70.02
3#	60	115.47	100	57.74
4#	55	122.08	100	70.02

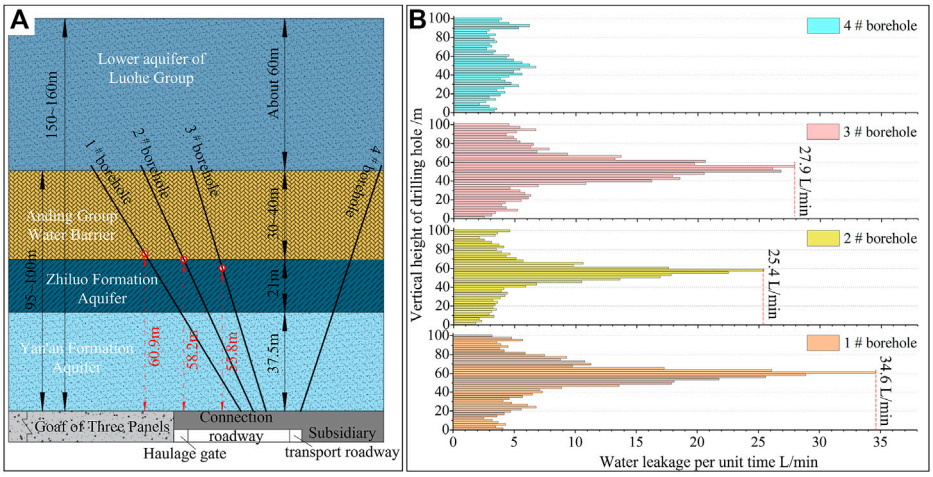

FIGURE 11
Upward hole segmented water injection method, **(A)** Borehole layout, **(B)** Unit time leakage water loss and borehole vertical height histogram.

distance of one working face length is spaced between two adjacent mining cycles, so that the cycle completes the design of the entire pan area recovery work, the calculated overburden hydraulic fracture development height is 58.45 m.

In order to verify the actual development height of the hydraulic fracture zone after the whole area has been re-mined, 2 months after the completion of filling and re-mining in the three pans, when the hydraulic fissure zone is fully developed to its maximum height, a drilling site is set up in the liaison road between the auxiliary transport roadway and the transport roadway on the outside of the stopping line of the first mining face in the three pans, and an inclined drilling hole is constructed in the direction of the goaf. Drill holes 1# to 3# are exploratory drill holes, avoiding the fall zone and penetrating diagonally to a certain height above the top boundary of the expected fissure zone. The drill hole 4# was drilled diagonally towards the coal pillar of the pan area and was a comparison drill hole not affected by mining. The parameters of drill holes 1–4# are shown in Table 1. The leakage per unit time of each section of borehole is measured by the method of segmented water injection into the inverted hole, and the development height of water flowing fractured zone is analyzed by the change of leakage. The borehole layout and the leakage per unit time are shown in Figure 11.

As shown in Figure 11, each section of 4# contrast borehole has different sizes of leakage, water injection leakage changes in the range of 2.1–6.7 L/min, in the drilling depth of 50–68 m and 110–113 m interval, the corresponding vertical height of 41–55.8 m, 90.2–92.6 m leakage showed two smaller peaks, the average leakage interval reached 5.64 L/min. The leakage in the contrast hole reflects the existence of primary cracks and certain permeability and water absorption when the rock layer is not broken and moved. The primary cracks and water absorption of the rock layer at the aquifer of Zhiluo Formation and the junction of the aquifuge of Anding Formation and the lower aquifer of Luohe Formation are larger than other rock layers. The net leakage can be obtained by subtracting the leakage of the corresponding section 4# background hole from the unit time leakage of each section of 1–3# borehole, so as to reduce the error caused by the primary fracture.

The maximum water loss per unit time of 1–3# boreholes is much larger than that of 4# comparative boreholes. The maximum

values are 34.6 L/min, 25.4 L/min and 27.9 L/min, respectively, and the corresponding vertical heights are 60.9 m, 58.2 m and 55.8m, respectively. It can be seen from the histogram of 1# hole leakage per unit time that when the vertical height is less than 19.5 m, the corresponding leakage is not much different from that of 4# contrast hole, indicating that the rock strata in this section may not be destroyed or in the compacted dense area. In the vertical height range of 19.5–60.9 m, the leakage shows an exponential upward trend until it reaches the maximum. This section should enter the water-conducting fracture zone, the gap is developed, and the rock mass is more damaged. After the vertical height of 60.9 m, the leakage decreases rapidly with the increase of the hole depth. After the vertical height of 65.5 m, the leakage has dropped below 10 L/min. The net leakage after subtracting the leakage of 4# contrast hole is less than 5 L/min on average. It shows that the development of water-conducting fractures caused by mining is small after the vertical height of 60.9 m.

The unit time leakage of 2# and 3# holes increases rapidly to the peak value from the vertical height of 41 m and 35 m respectively, and the distance to the fracture zone is farther than that of 1# hole. And the leakage volume decreases to 10 L/min near 77.1 m and 73.5 m deep (corresponding to a vertical height of 63 m) in both holes, which is about the junction of the water-bearing layer of the Zhiluo Formation and the water-insulating layer of the Anding Formation. This indicates that the development of the fracture has stopped below the water barrier of the Anding Group, and a comparison of the leakage in the latter part of the peak leakage per unit time in holes 2# and 3#, i.e., the leakage in the water barrier of the Anding Group, with the leakage in this section in the comparison holes also shows that the hydraulic fissures have not continued to develop upwards.

To sum up, through the comprehensive analysis of the leakage amount per unit time in 1–3# measurement boreholes and 4# comparison boreholes, it can be seen that the measured value of the development height of the hydraulic fissure zone in the whole area of the three pans after recovery is more in line with the calculated value, basically developing to the bottom of the water barrier of the stability group and stopping, none of them exceeds the safe hydraulic fissure zone height of 65 m.

6 Conclusion

(1) A model of the forces on the roof of a SCFM face was established to study the influence of two major controllable factors, namely the size of the working face and the infill rate, on the roof of an backfill coal mining face. The results show that the maximum tensile stress in the roof under the short-wall working face arrangement is more sensitive to the length of the working face than the filling rate, so the length of the working face should be the main factor in the design of the mining parameters to control the roof fracture development.

(2) Based on the elastic foundation coefficient, the length of the working face in a single mining cycle is designed. The whole SCFM process is always regarded as the process of controlling the deformation of the overlying strata by the three mining units of the current mining face and the left and right adjacent mining affected areas. Three basic structures composed of filling body, coal body and roof formed during a single mining cycle are constructed. Taking five working faces as examples, the stress of each step in a single mining cycle is analyzed. The results show that the fourth step of the mining cycle has the highest requirement for the working face interval. When the length of a single working face is designed to be 40 m, the roof control range of the three working units is greater than the stress concentration area.

(3) Taking the research mine as the engineering background, the layout of the SCFM working face in the whole area of the three panels was designed, and the development height of the water-conducting fracture under the condition of the whole mining area was calculated to be 58.45 m. Through the inverted hole water injection exploration method, it is verified that the actual development height of the water flowing fracture after mining and filling is close to the calculated value, and both exceed the safe height of 65 m.

Data availability statement

The original contributions presented in the study are included in the article/supplementary material, further inquiries can be directed to the corresponding author.

Author contributions

YY and ED wrote the manuscript. PJ and NZ revised the manuscript. YY and ED conducted the field experiments. YY, PJ, and NZ conceived the idea, carried out data analysis.

Funding

This work was funded by the Graduate Innovation Program of China University of Mining and Technology (grant number 2022WLKXJ048).

Acknowledgments

The authors would like to extend their thanks to the providers of the materials used in this study, and their appreciation to those who offered support for this study,

including CUMT and Coal Mining Branch, China Coal Research Institute.

Conflict of interest

The authors declare that the research was conducted in the absence of any commercial or financial relationships that could be construed as a potential conflict of interest.

Publisher's note

All claims expressed in this article are solely those of the authors and do not necessarily represent those of their affiliated organizations, or those of the publisher, the editors and the reviewers. Any product that may be evaluated in this article, or claim that may be made by its manufacturer, is not guaranteed or endorsed by the publisher.

References

Bai, E. H., Guol, W. B., Tan, Y., and Yang, D. M. (2018). The analysis and application of granular backfill material to reduce surface subsidence in China's northwest coal mining area. *PLoS One* 13, e0201112. doi:10.1371/journal.pone.0201112

Chen, L., Zhang, D. S., Fan, G. W., Zhang, S. Z., Wang, X. F., and Zhang, W. (2022). A new repeated mining method with preexisting damage zones filled for ultra-thick coal seam extraction - case study. *Front. Earth Sci.* 10, 1–14. doi:10.3389/feart.2022.835867

Chi, M. B., Zhang, D. S., Liu, H. L., Wang, H. Z., Zhou, Y. Z., Zhang, S., et al. (2019). Simulation analysis of water resource damage feature and development degree of mining-induced fracture at ecologically fragile mining area. *Environ. Earth Sci.* 78, 88. doi:10.1007/s12665-018-8039-5

Deng, X. J., Yuan, Z. X., Lan, L. X., De Wit, B. J., and Zhang, J. W. (2020). Roof movement and failure behavior when mining extra-thick coal seams using upward slicing longwall-roadway cemented backfill technology. *Adv. Mat. Sci. Eng.* 2020, 1–15. doi:10.1155/2020/5828514

Deng, X. J., Zhang, J. X., Zhou, N., De Wit, B., and Wang, C. T. (2017). Upward slicing longwall-roadway cemented backfilling technology for mining an extra-thick coal seam located under aquifers: A case study. *Environ. Earth Sci.* 76, 789. doi:10.1007/s12665-017-7120-9

Fan, L. M., Ma, X. D., Jiang, Z. Q., Sun, K., and Ji, R. J. (2019). Review and thirty years prospect of research on water-preserved coal mining. *Coal Sci. Technol.* 47, 1–30. doi:10.13199/j.cnki.cst.2019.07.001

Feng, J., Peng, H., Shuai, G., Meng, X., and Lan, L. X. (2017). A roof model and its application in solid backfilling mining. *Int. J. Min. Sci. Technol.* 27, 139–143. doi:10.1016/j.ijmst.2016.11.001

Feng, J., Wang, S. J., Hou, E. K., Ding, X., and Duan, H. J. (2021). Determining the height of water-flowing fractured zone in bedrock-soil layer in a jurassic coalfield in northern Shaanxi, China. *Adv. Civ. Eng.* 2021, 1–15. doi:10.1155/2021/9718802

Li, B. (2019). *Study on the characteristics of stress seepage of coal-rock mass and the influence of key strata under coal seam group mining with multiple protective layers*. Chongqing, China: Chongqing University. dissertation/doctor's thesis.

Li, M., Zhang, J. X., Deng, X. J., Ju, F., and Li, B. Y. (2017). Measurement and numerical analysis of water-conducting fractured zone in solid backfill mining under an aquifer: A case study in China. *Q. J. Eng. Geol. Hydrogeol.* 50, 81–87. doi:10.1144/qjegh2016-018

Li, M., Zhang, J. X., Jiang, H. Q., Huang, Y. L., and Zhang, Q. (2014). A thin plate on elastic foundation model of overlying strata for dense solid backfill mining. *J. China Coal Soc.* 39, 2369–2373. doi:10.13225/j.cnki.jccs.2013.1843

Li, X. B., Li, Q. S., Xu, X. H., Zhao, Y. Q., and Li, P. (2021). Multiple influence factor sensitivity analysis and height prediction of water-conducting fracture zone. *Geofluids* 2021, 1–10. doi:10.1155/2021/8825906

Liu, J. W., Sui, W. H., and Zhao, Q. J. (2017). Environmentally sustainable mining: A case study of intermittent cut-and-fill mining under sand aquifers. *Environ. Earth Sci.* 76, 562. doi:10.1007/s12665-017-6892-2

Liu, S. L., Li, W. P., and Wang, Q. Q. (2018). Height of the water-flowing fractured zone of the jurassic coal seam in northwestern China. *Mine Water Environ.* 37, 312–321. doi:10.1007/s10230-017-0501-1

Liu, Y., Yuan, S. C., Yang, B. B., Liu, J. W., and Ye, Z. Y. (2019). Predicting the height of the water-conducting fractured zone using multiple regression analysis and GIS. *Environ. Earth Sci.* 78, 422. doi:10.1007/s12665-019-8429-3

Miao, X. X., Cui, X. M., Wang, J. A., and Xu, J. L. (2011). The height of fractured water-conducting zone in undermined rock strata. *Eng. Geol.* 120, 32–39. doi:10.1016/j.enggeo.2011.03.009

Shen, Z. X., Zhang, Q., Chen, D. L., and Singh, V. P. (2021). Varying effects of mining development on ecological conditions and groundwater storage in dry region in Inner Mongolia of China. *J. Hydrol.* 597, 1–13. doi:10.1016/j.jhydrol.2020.125759

Tai, Y., Guo, S., and Lan, L. X. (2020). Reasonable gangue section length for disposing gangue pollutants in the new green mixed workface. *Bull. Eng. Geol. Environ.* 79, 1669–1682. doi:10.1007/s10064-019-01677-x

Wang, G. (2015). *Developing law of water-flowing fracture with wongawilli backfill in coal mines*. Beijing China: China university of mining and technology. dissertation/master's thesis.

Wang, X. F., Zhang, D. S., Sun, C. D., and Wang, Y. (2016). Surface subsidence control during bag filling mining of super high-water content material in the Handan mining area. *Int. J. Oil, Gas. Coal Technol.* 13, 87–102. doi:10.1504/ijogct.2016.078049

Wen, J. H., Cheng, W. M., Chen, L. J., Shi, S. S., and Wen, Z. J. (2019). A study of the dynamic movement rule of overlying strata combinations using a short-wall continuous mining and full-caving method. *Energy Sci. Eng.* 7, 2984–3004. doi:10.1002/ese3.474

Wen, P., Guo, W. B., Tan, Y., Bai, E. H., Ma, Z. B., Wu, D. T., et al. (2022). Paste backfilling longwall mining technology for thick coal seam extraction under buildings and above confined aquifers: A case study. *Minerals* 12, 470. doi:10.3390/min12040470

Xie, X. S., Hou, E. K., Wang, S. M., Sun, X. Y., Hou, P. F., Wang, S. B., et al. (2021). Formation mechanism and the height of the water-conducting fractured zone induced by middle deep coal seam mining in a sandy region: A case study from the xiaobaodang coal mine. *Adv. Civ. Eng.* 2021, 1–11. doi:10.1155/2021/6684202

Xu, Y. J., Ma, L. Q., Ngo, I., and Zhai, J. T. (2022). Prediction of the height of water-conductive fractured zone under continuous extraction and partial backfill mining method-A case study. *Sustainability* 14, 6582. doi:10.3390/su14116582

Yao, Q. L., Zheng, C. K., Tang, C. J., Xu, Q., Chong, Z. H., and Li, X. H. (2020). Experimental investigation of the mechanical failure behavior of coal specimens with water intrusion. *Front. Earth Sci.* 7, 1–13. doi:10.3389/feart.2019.00348

Zhang, J. X., Jiang, H. Q., Deng, X. J., and Ju, F. (2014). Prediction of the height of the water-conducting zone above the mined panel in solid backfill mining. *Mine Water Environ.* 33, 317–326. doi:10.1007/s10230-014-0310-8

Zhang, Y., Cao, S. G., Zhang, N., and Zhao, C. Z. (2020). The application of short-wall block back fill mining to preserve surface water resources in northwest China. *J. Clean. Prod.* 261, 121232. doi:10.1016/j.jclepro.2020.121232

Zhang, Y., Liu, Y. Z., Lai, X. P., and Gao, J. M. (2021). Physical modeling of the controlled water-flowing fracture development during short-wall block backfill mining. *Lithosphere* 2021, 1–15. doi:10.2113/2021/2860087

Zhao, H. F., Wang, X. H., Liu, Z. Y., Yan, Y. J., and Yang, H. X. (2018). Investigation on the hydraulic fracture propagation of multilayers-commingled fracturing in coal measures. *J. Pet. Sci. Eng.* 167, 774–784. doi:10.1016/j.petrol.2018.04.028